Title: Simultaneous dual recordings from hair cells and their calyx afferents reveal the functional significance of these specialized endings in the vestibular periphery.

Running title: Three modes of synaptic transmission between vestibular Type I hair cells and calyx afferents

Authors: Donatella Contini[1], Gay R. Holstein[2,3] and Jonathan J. Art[1]

[1]Department of Anatomy & Cell Biology, University of Illinois College of Medicine, 808 S. Wood St, Chicago, IL 60612, USA. [2]Neurology and [3]Neuroscience, Icahn School of Medicine at Mount Sinai, 1468 Madison Ave, New York, NY 10029, USA.

Corresponding Author: jart@uic.edu

Abstract

In the vestibular periphery, transmission via conventional synaptic boutons is supplemented by postsynaptic calyceal endings surrounding Type I hair cells. This review focusses on the multiple modes of communication between these receptors and their enveloping calyces as revealed by simultaneous dual electrode recordings. Classic orthodromic transmission is facilitated and supplemented by two forms of bidirectional communication enabled by the extensive cleft between the Type I hair cell and its calyx. The slowest mode of transmission occurs over tens of milliseconds: potassium ions accumulate in the synaptic cleft, depolarizing both the hair cell and afferent to potentials allowing rapid vesicle fusion in the receptor and large excitatory postsynaptic potentials that trigger action potentials in the afferent. On the millisecond timescale, conventional glutamatergic quantal transmission occurs when hair cells are depolarized to potentials sufficient for calcium influx and vesicle fusion. A third form of transmission occurs over tens of microseconds, resulting from the large voltage- and ion-sensitive cleft-facing conductances in both the hair cell and the calyx that are open at their resting potentials. Current flowing out of either the hair cell or the afferent divides into the fraction flowing across the cleft into its cellular partner, and the remainder flowing out of the cleft and into the surrounding fluid compartment. These findings suggest multiple biophysical bases for the extensive repertoire of response dynamics seen in the population of primary vestibular afferent fibers. The results further suggest that evolutionary pressures drive selection for the calyx afferent.

Key words: synaptic transmission, hair cell, calyx, ion accumulation, quantal transmission, nonquantal transmission, ephaptic transmission, resistive coupling, vestibular

Introduction

A persistent question in the vestibular field is the functional significance of specialized calyx endings present on a subset of primary afferents in vestibular end organs. A majority of afferent and all efferent synapses involving hair cells (HCs) in the labyrinth, as well as the cochlea are mediated by conventional bouton endings. While the calyx represents a unique characteristic distinguishing vestibular from auditory sensory epithelia, the function of this morphologically specialized synapse remains obscure. Recent dual simultaneous recordings from HCs and their associated calyx afferents demonstrate that there are three modes of intercellular communication between them. In addition to unidirectional quantal transmission between HCs and afferents, there are two bidirectional forms of transmission. The slower of the two results from potassium flux into the cleft from either HC or afferent over tens of milliseconds. The resulting $[K^+]_{cleft}$ changes the potassium equilibrium potential for channels facing the cleft. The more rapid form of transmission results from HC and afferent channels open near their respective resting potentials. These allow current flowing into the cleft from either HC or afferent to divide between a component that flows out of the cleft near its apex at the neck of the Type I HC and a component that flows across the cleft into the synaptic partner. As yet, there is no compelling evidence that the calyx ending is uniquely associated with particular characteristics of afferent discharge regularity or dynamics.

Anatomy, synaptic morphology, and innervation

With the advent of amniotes, the vestibular epithelia evolved to contain two subtypes of HC receptors. These were initially differentiated on the basis of HC cytology alone, and were subsequently defined by morphological differences in their associated afferent processes as well (1). Type I HCs are flask-shaped and are innervated by an afferent chalice surrounding the entire basolateral surface of the HC except the apical neck. The extensiveness and exclusivity of the cleft between the HC and its enveloping calyx, together with the tight junction seal protecting the endolymphatic space, creates a unique, diffusion-limited, femtoliter environment that is markedly different from the perilymph. Type II HCs are cylindrical and participate in comparatively small synapses involving bouton-like endings of vestibular nerve fibers that terminate on both the receptor somata and the outer calyceal faces (2, 3).

In vestibular epithelia, both HC types utilize ribbon synapses for quantal transmission. These structures were originally observed in retinal photoreceptors, in which they resemble a folded ribbon located several nanometers from the presynaptic membrane. The ribbon was bedecked with synaptic vesicles, with a few of these attached to the cell's plasma membrane (4-8). Subsequent studies revealed variability in the overall structure, ranging from ribbons to spheres, ovals, plates, and bars (9, 10). This led to the adoption of a more general term "synaptic body" to describe the configuration of synaptic vesicles tethered to a central structure with a minority docked at an active zone.

To date, synaptic bodies have been reported in retinal photoreceptors and bipolar cells, pinealocytes, electroreceptors, and auditory and vestibular HCs (9). The size, shape, orientation, configuration, and membrane linkage of the synaptic body vary, as do the number, density, tethering and docking of the associated synaptic vesicles (10, 11). In auditory HCs, this morphological diversity has been correlated with functional differences in peripheral auditory

signal processing based on Ca^{2+}-dependent exocytosis (12, 13). In both vestibular and auditory HCs, ribbon synapse morphology is thought to underlie the ability of HCs to respond with graded, high rates of sustained quantal transmitter release (14, 15), but see (16). This dual function is achieved by the orchestrated availability of docked vesicles for immediate rapid exocytosis, and tethered vesicles (the "readily releasable pool") poised for imminent release (17, 18). As shown in Fig 1, ribbon synapses are present at Type I HC synapses with calyces, and Type II HC synapses with both boutons and calyx outer faces (2, 3, 19, 20). Efferent synapses with afferents and Type II HCs display conventional presynaptic membrane specializations and postsynaptic subsynaptic cisterns in the HCs. Despite this well-defined anatomy, however, the precise role of the calyx in shaping HC-afferent signaling is not known. In that context, it is noteworthy that Wersäll reportedly regretted his sequential naming of the HCs, deeming the Type I HC-calyx architecture more highly evolved (21).

Morphophysiology

Decades of effort has focused on mapping morphological attributes of vestibular end organs and correlating these maps with dynamics and statistics of afferent firing (22-30); (Review: (31)). Based on intracellular recordings, dye injections and light microscopic morphological reconstructions (32, 33), the crista ampullaris in multiple species has been subdivided into concentrically or linearly organized zones that evince differences in HC demographics and afferent innervation patterns (34, 35) (Fig. 1D). The posterior canal crista of turtles, for example, is organized into two symmetrical hemicristae separated by a central torus (36, 37). Each hemicrista has a central zone surrounded by a peripheral area that extends toward the torus and planum. All afferents in the central zone have calyces, manifest as either calyx-only fibers (33, 34) or dimorphic (38) fibers having both calyx and bouton endings. Afferents with bouton terminals are present in the peripheral zones throughout the crista, but more densely populate the zone with larger afferent fibers nearest the torus (33). Reflecting this, Type I HCs are more prevalent in the central zone while Type II HCs are present throughout the crista.

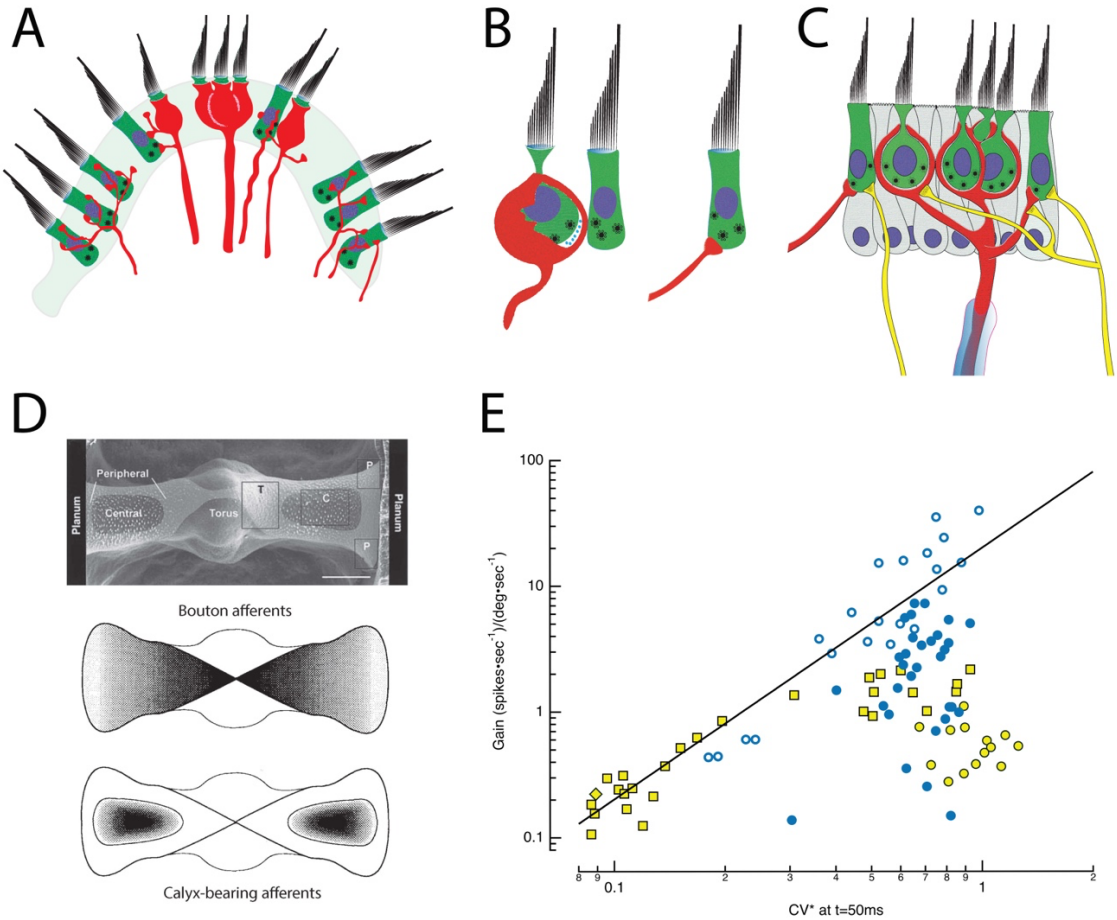

Figure 1. Morphophysiology of the semicircular canal (SCC) epithelium. A. Cross section through the saddle-shaped crista reveals distinct innervation patterns: boutons are found peripherally, with calyx and dimorphic afferents located centrally (adapted from (33)). B. Type I HCs are internal to an enveloping calyx that creates an extensive synaptic cleft in which ions accumulate. Type I HCs have synaptic bodies associated with quantal transmission onto the inner leaflet of the calyx. Type II HCs also have synaptic bodies indicative of quantal transmission and synapse onto bouton endings (right), or onto the outer leaflet of an afferent calyx (middle and left). C. A single myelinated afferent (red) may branch into several calyces, each containing one or more Type I HCs. Additional input from Type II HCs may occur via synapses onto the outer face of the afferent (left), or through bouton endings of fine collateral branches (right). Efferent fibers (yellow) from the brainstem synapse on HCs and on the outer faces of calyces (39). D. Top: SEM plan view of the turtle posterior semicircular canal crista (40). The epithelium is divided into two hemicristae with central and peripheral regions that extend bilaterally from the torus to the planum on either side. Middle: Map of the density of bouton afferents in each hemicrista. Bottom: Density map of the distribution of calyx-bearing afferents in the central regions of each hemicrista (37). E. Afferent signaling dynamics and discharge statistics in the posterior SCC of chinchilla (yellow symbols) (32) and turtle (blue symbols) (33) are correlated and map systematically across the epithelium. CV*, a measure of the irregularity of the interval between successive APs, is a continuous variable with the most regular fibers on

the left and the most irregular on the right. Typically, when either animal was examined with low-frequency, 0.3 or 2 Hz, rotations, low gain afferents sensitive to velocity are more regular, and high gain afferents are sensitive to accelerations. For the chinchilla, the low gain bouton (yellow diamond) and dimorphic (yellow square) afferents demonstrate that regular discharge can be achieved with either bouton or calyx endings. Data seen on the right side, including high gain bouton (turtle: blue, open circle) and dimorphic (turtle: blue, filled circle; chinchilla: yellow square) fibers demonstrate that irregular discharge can be achieved by afferents containing either type of ending. The irregular low gain "calyx only" afferents in chinchilla (yellow filled circle) remain a puzzle but may simply be afferents that respond maximally to stimulations of higher-frequencies (41) or vibration (42). CV* for chinchilla data transformed from 15 ms inter-spike interval (ISI) CV* to that at 50 ms ISI using a third-order polynomial fit to the CV* vs ISI data at 50 ms in Fig. 1 of (32), equivalent to CV* and ISI used in the turtle data (33).

This differential localization of HCs and afferent endings across the crista underlies a coherent physiological and functional map of afferent activity (32, 34, 43-47). Specifically, the regularity of afferent fiber discharge, defined by the variability in time between sequential action potentials (APs) reportedly is a continuous variable that correlates with the fiber's response to velocity or angular acceleration (48-51). Regular afferents have evenly spaced spontaneous firing rates and respond to low frequency angular motion with tonic discharge. In effect, this mathematically integrates the acceleration stimulus, transmitting signals that are proportional to head velocity. In contrast, the spontaneous firing of irregular afferents shows high variability in the timing between APs. Angular acceleration elicits phasic, dynamic responses from these fibers, which more closely resemble the accelerative stimulus. Moreover, regularly discharging fibers as a group have lower gain (spikes*sec^{-1}/degrees*sec^{-1}) than irregular afferents. In turtles, low gain, regularly-firing bouton afferent endings sensitive to velocity are concentrated near the planum, while higher gain bouton afferents sensitive to acceleration terminate closer to the torus (52). In contrast, most calyx-bearing fibers, which end in the central zone, are irregular afferents. The sensitivity of these fibers to low-frequency rotation varies over two orders of magnitude and is not strictly correlated with the degree of irregularity of the spontaneous discharge rate. Nevertheless, an integrated morphophysiological map of the crista emerges in which low gain, regularly discharging, velocity-sensitive bouton afferents terminate nearest the planum, bouton afferents of higher gain and more irregular discharge terminate nearest the torus, and calyx-bearing, irregularly-firing units terminate in the central zone of each hemicrista (Fig. 1D). Functionally, the high gain fibers across species are particularly attuned to acceleration (52) or to jerks, the derivative of acceleration (53), and rapidly saturate as the amplitude of the stimulus increases. Medium gain afferents remain active over a wider motion spectrum, while low gain fibers are not prone to saturate, regardless of the magnitude of the head acceleration (Fig. 1E). One caveat to this characterization is that the afferent gains were typically assessed at single low frequencies of stimulation (32, 33), although the most irregular fibers are often maximally responsive to higher frequencies and even vibrational or sound stimuli (41, 54, 55).

Based on the initial correlation of afferent terminal distribution with regularity of spontaneous firing and response dynamics, significant effort was directed toward identifying

173 causality. It remained to be determined whether the regularity of a fiber's spontaneous firing
174 derived from the geographical position of its terminals in the crista, or from the specific array of
175 HC inputs to trunk, branch, and twig segments of the parent process. Studies addressing this
176 have been useful in highlighting the overall importance of regional localization in the crista and
177 suggesting the type of HCs, three-dimensional terminal architecture and synapses contributing
178 to individual afferent responses. However, efferent innervation (56-60), GABA-mediated
179 modulation of glutamatergic transmission (61-63), ion accumulation in the synaptic cleft (39,
180 64-66), and Type II HC input to the external face of the calyx (3, 67) have not been incorporated
181 into these analyses. Since each of these has the potential to markedly alter peripheral
182 vestibular activity, conclusions from these studies are necessarily tentative.
183
184 **Solitary cells**
185 To supplement information gleaned by morphophysiology, currents were analyzed from
186 HCs classified as Type I or II based on their amphoral or cylindrical profile (66, 68-86), from
187 identified regions of the epithelia (40). This approach emulated a strategy used in lower
188 vertebrates to demonstrate that the kinetics of voltage- and ion-sensitive basolateral channels
189 imparted frequency selectivity to solitary auditory HCs (87-93). Typically, solitary vestibular HCs
190 were bathed in artificial perilymph, an ionic environment appropriate for Type II cells, but of
191 unknown propriety for the ionically dynamic environment of a Type I HC and its calyx. In
192 principle, such a bath would be apposite for isolating conductances based on their voltage
193 ranges of activation, kinetics, ionic permeabilities, and pharmacological profiles. In artificial
194 perilymph however, analysis of fundamental metrics such as I-V curves would be altered by
195 driving forces reflecting equilibrium potentials for each ion when bathed in high sodium and
196 low potassium. The vestibular potassium channels characterized in this way have been
197 reviewed (94). A startling discovery was that Type I HCs possess a low-voltage outward-
198 rectifying potassium current, $IK_{(LV)}$, that activates at very hyperpolarized potentials. Its full
199 activation near the HC resting potential was considered problematic, since enormous
200 transduction currents would be required to depolarize a cell to potentials necessary for the
201 calcium influx and vesicle fusion associated with quantal transmission. A solution to this
202 paradox was proposed by Chen (95) who suggested that potassium accumulation in the
203 synaptic cleft between the HC and calyx was analogous to the potassium accumulation in
204 tissues surrounding the squid giant axon (96), and that potassium flowing from the HC would
205 increase $[K^+]_{cleft}$ and depolarize E_K for HC and afferent conductances facing the cleft. As a result,
206 the Type I HC would be depolarized to potentials necessary for calcium influx and quantal
207 transmission, but the increased $[K^+]_{cleft}$ would also depolarize the calyx.
208
209

210 **Theoretical and single-electrode studies**

211 Theoretical and experimental approaches were then used to examine the Chen conjecture.
212 The theoretical analysis (97, 98) relied on equivalent circuits of the Type I HC, cleft, and calyx to
213 analyze the problem primarily as ephaptic transmission (99-101) embellished by potassium
214 accumulation. In general, this analysis concluded that the potential drops associated with
215 current flow along the cleft from HC base to apex created only minor differences in the driving
216 force for channels facing the cleft, and as a result were not likely to be a major source of
217 coupling (98), but see (102). The possibility that ion accumulation could have the effect
218 suggested by Chen was also examined experimentally (103). Following blockade of quantal
219 transmission, slow potentials that were phase-locked to the stimulus could be detected, a
220 phenomenon consistent with ion accumulation. Two groups examined the potassium
221 accumulation question by perforating the calyx and patch-recording from the enveloped Type I
222 HCs *in situ* (104-106). These experiments demonstrated that depolarization of either the HC or
223 the calyx caused a reversal of the HC potassium tail currents, suggesting an elevation of $[K^+]_{cleft}$
224 consistent with Chen's conjecture. Such studies, together with one suggesting a transmitter role
225 for protons (65), yielded results in which the interactions/coupling between cells occurred over
226 tens of milliseconds. However, experiments using mechanical stimulation of the HC bundle
227 demonstrated that when quantal transmission was blocked, the HC-afferent coupling could be
228 extremely rapid, which would facilitate transmission of high frequency information (107, 108).
229 Such contradictory viewpoints evoke the Indian parable of blind men describing an elephant
230 (109), where each detects and interprets a small part of the more complex whole. This led to a
231 quest to discover underlying biophysical mechanisms that could reconcile the differing results.
232

233 **Dual-electrode studies**

234 The demonstration that $[K^+]_{cleft}$ can be increased by potassium fluxes from either synaptic
235 partner is a reminder that interpretations of single-electrode voltage-clamp studies of either HC
236 or afferent alone can be problematic. The privileged ionic compartment created by the
237 apposition between a HC and calyx means that any single-electrode study that voltage clamped
238 one cell necessarily allowed the potential of the other cell to vary freely. Moreover, studies that
239 patched onto Type I HCs *in situ* (104-108) did so by perforating the calyx, and there is ample
240 evidence that this approach compromises the cleft environment and results in two types of
241 recordings: those similar to solitary cells bathed in perilymph, and those in which reversal of the
242 potassium tail currents demonstrate an increase in $[K^+]_{cleft}$ (104, 105).

243 To address this, we developed an approach to simultaneously patch the HC and calyx
244 without breaching the calyceal membranes (39, 64). In essence, this requires patching the HC
245 either on its apex or on the exposed 2 – 3μm of its basolateral wall extending apically above the
246 enveloping calyx. With this approach, the potentials of both cells can be interrogated or
247 controlled in current clamp or voltage clamp, leaving the cleft ionic environment intact. Our
248 initial studies (39) focused on ion accumulation and used the reversal potential of the HC
249 potassium tail currents following depolarization to track E_K and estimate $[K^+]_{cleft}$. Blocking HC
250 potassium flux abolished slow coupling over tens of milliseconds but spared quantal
251 transmission. Our subsequent study (64) demonstrated that HC potassium flux depended upon
252 the activation of both voltage-activated and calcium-activated potassium channels, and that the

253 voltage-activated conductance was sensitive to $[K^+]_{cleft}$ and $[Ca^{2+}]_{cleft}$. Clamping $[H^+]_{cleft}$ resulted
254 in stronger coupling between the two, suggesting that H^+ was not a primary transmitter acting
255 through acid-sensitive ion channels. Pharmacological experiments using an HCN channel
256 blocker (39) demonstrated that, in addition to synaptic coupling acting through HC and afferent
257 potassium channels, the elevated $[K^+]_{cleft}$ not only decreased outward K^+ flux through calyceal
258 voltage-sensitive potassium channels, but also shifted the activation curve of G_{HCN} (85), creating
259 a depolarizing inward flux of Na^+ and K^+ through the HCN channels. These potassium-sensitive
260 effects obtained regardless of whether the increased $[K^+]_{cleft}$ was due to HC or to afferent fluxes.
261 Inward transduction currents would generate an outward flow of K^+ through the basolateral HC,
262 elevate $[K^+]$ and shift E_K, causing depolarization of both HC and afferent (Fig 2A). This would
263 lead to additional Ca^{2+} influx and vesicle fusion, resulting in quantal glutamatergic transmission
264 to calyx AMPARs. Taken together, these results provide strong support for Chen's conjecture
265 that potassium accumulation in the cleft facilitates quantal transmission between a Type I HC
266 and calyx. For complex calyces with more than one enveloped HC, the findings indicate that
267 depolarization of one HC can depolarize the afferent, which would then depolarize neighboring
268 receptors enveloped by the shared afferent (Fig. 2A). In that light, slow potassium accumulation
269 represents bidirectional synaptic coupling that acts over tens of milliseconds.
270 One remarkable result of these experiments (64) was a demonstration that there is also a
271 rapid bidirectional coupling between the cells that allows currents to activate within
272 microseconds of depolarization. With depolarization near the HC and calyx resting potentials,
273 there are a significant number of ion channels with high open probabilities. Rapid inward
274 transduction current would immediately flow out through HC channels, with much of the
275 current flowing into the extensive synaptic cleft and a minority flowing into the calyx (Fig. 2B).
276 Such coupling can be analyzed using either Kirchhoff's current or voltage laws, and the
277 conclusion is the same: there would be relatively small voltage gains or drops of a few mV along
278 the cleft depending on the current direction and the precise resistance (98, 102). The impact of
279 this on specific channels facing the cleft is unknown and would greatly depend on their position
280 with respect to the apical gap between HC and calyx. The dual recordings allow us to measure
281 the current flow out of one synaptic partner and into the other (39, 64) (Fig. 2B, C). Such rapid
282 current flow from HC into calyx, Fig. 2B, may underlie the rapid transmission of high frequency
283 mechanical stimuli (107, 108, 110), and may be the substrate for detection of sound and
284 vibration (27, 42, 55, 111-116). As with slow potassium accumulation, this rapid ion flow
285 through open channels is bidirectional, as evidenced by the retrograde transmission of calyx
286 afferent APs into the HC (Fig. 2C) (39).
287 Dual recordings also provided the incidental observation that in the central region, the EPSCs
288 from Type I HCs onto the calyx inner leaflet were small (39, 117, 118), whereas those from
289 Type II HCs onto the outer leaflet (39) were as large as those reported in the cochlea (14), and
290 would be sufficient to trigger APs in afferents near the spike threshold. This highlights the risk
291 of morphophysiological studies defining calyx-only afferents solely using light microscopy.
292
293

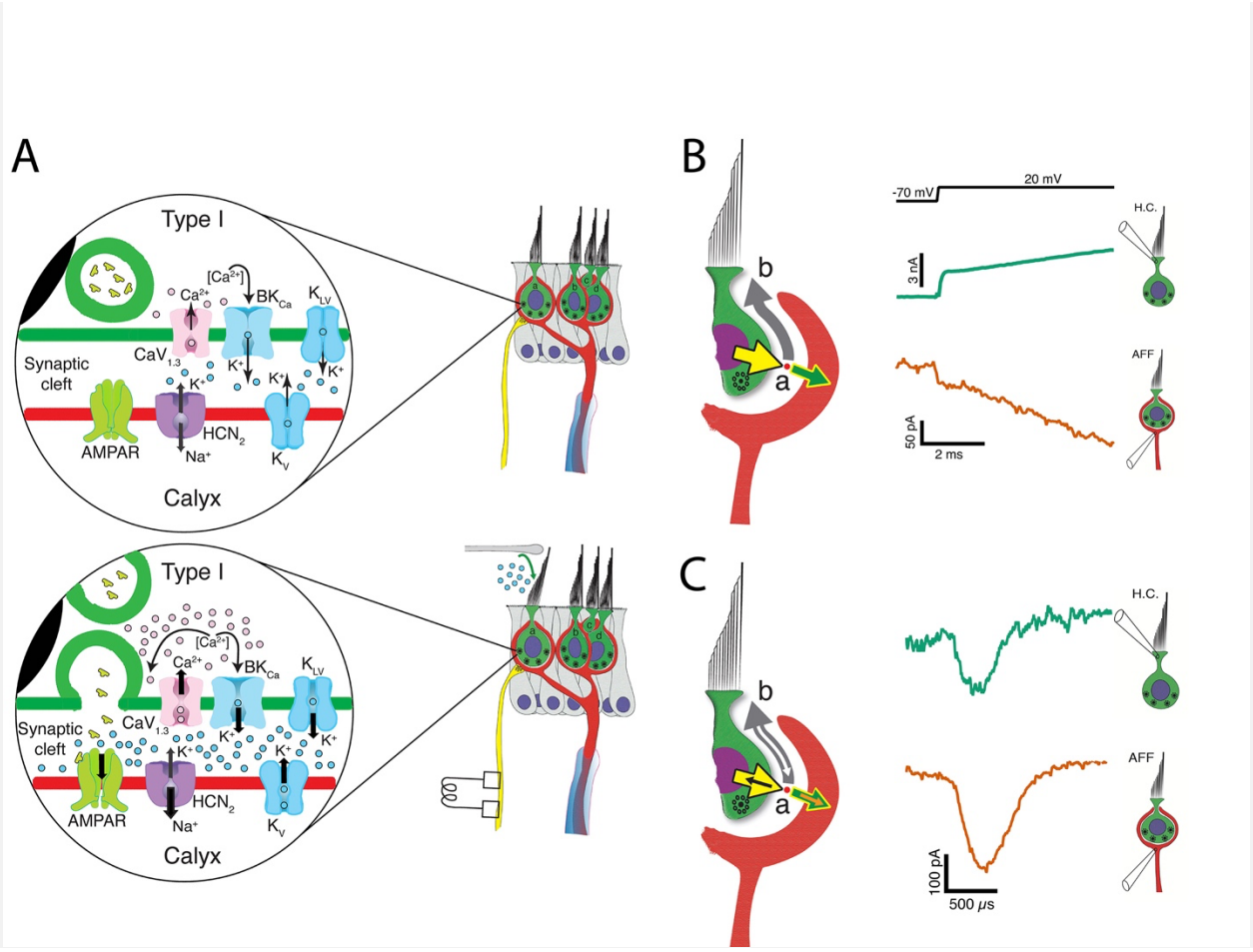

Figure 2. Three forms of synaptic transmission between Type I HC and calyx afferent. A. In the absence of mechanical stimulation (upper panel), basolateral potassium currents activated at hyperpolarized potentials elevate the $[K^+]_{cleft}$ to concentrations slightly greater than that in perilymph. This results in a shift in E_K and depolarization of the HC to its resting potential. At rest there is occasional vesicle fusion and the production of a background rate of afferent discharge. Upon mechanical stimulation (lower panel), the inward transduction current flows into the HC and out the basolateral conductances into the cleft as a potassium current. This further increases $[K^+]_{cleft}$ and further depolarizes E_K for conductances in the HC and afferent membranes facing the cleft. The HC depolarization gates Ca^{2+} influx, resulting in fusion of synaptic vesicles and quantal transmission of glutamate to AMPARs on the calyx inner leaflet. The slow accumulation of potassium thereby facilitates quantal transmission near the resting potential. It is likely that the irregularities of vesicle fusion and large quanta that initiate an AP are driven by neighboring Ca-channel noise (119), and as a consequence the degree of regularity of afferent discharge would be determined by the degree to which the post-synaptic afferent conductances have intrinsic memory and oscillatory behavior similar to those found in HCs of the turtle auditory papilla (91, 120). B. Large conductances in the HC and calyx near the resting potential also create an open resistive pathway between the two that permits a fraction of the transduction current to be communicated across the cleft and into the calyx without synaptic delay. Outward current from the HC (yellow arrow) divides at point (a) into a large

component (gray arrow) going along the cleft into the bath at point (b), and a smaller current flowing into the calyx (green arrow). The measured current for the HC (bluish-green current trace) and calyx (vermillion trace) show transmission within 10 µs. C. Resistive coupling can also be demonstrated during large HC depolarizations that depolarize the calyx to potentials sufficient to generate an AP that travels into the calyx. Currents due to the invasion of an AP will sum with the primary currents illustrated in B. With an AP, an additional inward current (orange arrow) flows into the calyx, with an amplitude equal to the sum of the corresponding currents flowing into the HC (black arrow) and down the cleft (white arrow). The coupling between the calyx retrograde AP current (vermillion) and the induced HC current (bluish-green) is 12 µs (modified from (64)).

Conclusions

During vertebrate evolution, selective pressures favored increased sensitivity and flawless encoding of high-frequency three-dimensional vestibular information. This correlated with a higher prevalence of Type I HCs and calyx afferents (121, 122, 123, 134), which exhibit unidirectional quantal and two forms of bidirectional communication. From an evolutionary perspective, the pressure for rapid communication is best served by direct resistive/electrical coupling facilitated by large HC and afferent conductances present at their resting potentials. These conductances would make it difficult for HC transduction currents to depolarize HCs to potentials necessary for calcium influx, vesicle fusion and quantal transmission, a process that would be an absolute requirement during evolution until the appearance of protocalyces. At each stage of calyx expansion, cleft-facing conductances would elevate $[K^+]_{cleft}$, depolarize E_K to facilitate quantal transmission, and provide a resistive path between synaptic partners. While not as complete an association as that between an invertebrate HC and its axon, or that of gap junctions typical of electrical synapses, the resistive coupling between HC and calyx has minimal delay, is dynamic, and would increase as mechanical inputs become larger.

Author contributions

All authors have made a substantial, direct, and intellectual contribution to the work and approved it for publication.

Funding

This work was supported by US HHS, NIH, National Institute on Deafness and Other Communication Disorders, grants R21 DC017292; R21 DC017577, R01 DC019953, and R01 DC008846

Acknowledgements

We would like to thank Professor A. Brichta for graciously allowing us to modify, reuse, and repurpose his figures in Figure 1.

References

1. Wersäll J. Studies on the structure and innervation of the sensory epithelium of the cristae ampullares in the guinea pig. *Acta Otolaryngology Suppliment (Stockh)* (1956) 126:7-85.
2. Goldberg JM, Lysakowski A, Fernández C. Morphophysiological and ultrastructural studies in the mammalian cristae ampullares. *Hear Res* (1990) 49(1-3):89-102. Epub 1990/11/01.
3. Lysakowski A, Goldberg JM. Ultrastructural analysis of the cristae ampullares in the squirrel monkey (Saimiri sciureus). *J Comp Neurol* (2008) 511(1):47-64. Epub 2008/08/30. doi: 10.1002/cne.21827.
4. Sjöstrand FS, editor. The Ultrastructure of the Retinal Rod Synapses of the Guinea Pig Eye. *Proceedings of the Electron Microscope Society of America*; 1953: Journal of Applied Physics (1953).
5. De Robertis E, Franchi CM. Electron microscope observations on synaptic vesicles in synapses of the retinal rods and cones. *J Biophys Biochem Cytol* (1956) 2(3):307-18. Epub 1956/05/25. doi: 10.1083/jcb.2.3.307.
6. Carasso N. Etude au microscope électronique des synapses des cellules visuelles chez le têtard d'Alytes obstetricans. [Electron microscopy of the synapses of the visual cells in the tadpole of Alytes obstetricans]. *Comptes rendus hebdomadaires des séances de l'Académie des sciences D, Sciences naturelles* (1957) 245(2):216-9. Epub 1957/07/08.
7. Polyak SL. *The Retina*. Chicago: The University of Chicago Press (1941).
8. Sjostrand FS. Ultrastructure of retinal rod synapses of the guinea pig eye as revealed by three-dimensional reconstructions from serial sections. *J Ultrastruct Res* (1958) 2(1):122-70. Epub 1958/11/01. doi: 10.1016/s0022-5320(58)90050-9.
9. Sterling P, Matthews G. Structure and function of ribbon synapses. *Trends Neurosci* (2005) 28(1):20-9. doi: 10.1016/j.tins.2004.11.009.
10. Moser T, Brandt A, Lysakowski A. Hair cell ribbon synapses. *Cell Tissue Res* (2006) 326(2):347-59. Epub 2006/09/01. doi: 10.1007/s00441-006-0276-3.
11. Schmitz F. The making of synaptic ribbons: how they are built and what they do. *Neuroscientist* (2009) 15(6):611-24. Epub 2009/08/25. doi: 10.1177/1073858409340253.
12. Johnson SL, Forge A, Knipper M, Munkner S, Marcotti W. Tonotopic variation in the calcium dependence of neurotransmitter release and vesicle pool replenishment at mammalian auditory ribbon synapses. *J Neurosci* (2008) 28(30):7670-8. doi: 10.1523/JNEUROSCI.0785-08.2008.
13. Meyer AC, Frank T, Khimich D, Hoch G, Riedel D, Chapochnikov NM, et al. Tuning of synapse number, structure and function in the cochlea. . *Nature Neurosci* (2009) 12:444–53.
14. Glowatzki E, Fuchs PA. Transmitter release at the hair cell ribbon synapse. *Nat Neurosci* (2002) 5(2):147-54. Epub 2002/01/22. doi: 10.1038/nn796.
15. Fuchs PA, Glowatzki E, Moser T. The afferent synapse of cochlear hair cells. *Curr Opin Neurobiol* (2003) 13(4):452-8. Epub 2003/09/11.
16. Holt JC, Xue JT, Brichta AM, Goldberg JM. Transmission between type II hair cells and bouton afferents in the turtle posterior crista. *J Neurophysiol* (2006) 95(1):428-52. Epub 2005/09/24. doi: 10.1152/jn.00447.2005.
17. von Gersdorff H, Matthews G. Electrophysiology of synaptic vesicle cycling. *Annu Rev Physiol* (1999) 61:725-52. doi: 10.1146/annurev.physiol.61.1.725.

18. Holt M, Cooke A, Neef A, Lagnado L. High mobility of vesicles supports continuous exocytosis at a ribbon synapse. *Curr Biol* (2004) 14:173–83.
19. Lysakowski A, Goldberg JM. A regional ultrastructural analysis of the cellular and synaptic architecture in the chinchilla cristae ampullares. *J Comp Neurol* (1997) 389(3):419-43. Epub 1997/12/31.
20. Lysakowski A. Synaptic organization of the crista ampullaris in vertebrates. *Ann N Y Acad Sci* (1996) 781:164-82.
21. Engström H. The first-order vestibular neuron. In: Graybiel A, editor. *Symposium on the role of the vestibular organs in space exploration NASA SP-187*. Washington DC: National Academies (1970). p. 123-35.
22. Goldberg JM, Fernández C. Vestibular mechanisms. *Annu Rev Physiol* (1975) 37:129-62. Epub 1975/01/01. doi: 10.1146/annurev.ph.37.030175.001021.
23. Suzuki M, Harada Y. An experimental study on the frog semicircular canal--functions of cupula and vestibular ganglion. *J Otolaryngol* (1985) 14(1):36-40.
24. Suzuki M, Harada Y. An experimental study on the physiological significance of the mode of cupular movement. *Arch Otorhinolaryngol* (1985) 242(1):57-62.
25. Rabbitt RD, Boyle R, Highstein SM. Sensory transduction of head velocity and acceleration in the toadfish horizontal semicircular canal. *J Neurophysiol* (1994) 72(2):1041-8.
26. Hullar TE, Della Santina CC, Hirvonen T, Lasker DM, Carey JP, Minor LB. Responses of irregularly discharging chinchilla semicircular canal vestibular-nerve afferents during high-frequency head rotations. *J Neurophysiol* (2005) 93(5):2777-86. doi: 10.1152/jn.01002.2004.
27. Curthoys IS, Kim J, McPhedran SK, Camp AJ. Bone conducted vibration selectively activates irregular primary otolithic vestibular neurons in the guinea pig. *Exp Brain Res* (2006) 175(2):256-67. doi: 10.1007/s00221-006-0544-1.
28. Lasker DM, Han GC, Park HJ, Minor LB. Rotational responses of vestibular-nerve afferents innervating the semicircular canals in the C57BL/6 mouse. *J Assoc Res Otolaryngol* (2008) 9(3):334-48. doi: 10.1007/s10162-008-0120-4.
29. Jamali M, Sadeghi SG, Cullen KE. Response of vestibular nerve afferents innervating utricle and saccule during passive and active translations. *J Neurophysiol* (2009) 101(1):141-9. doi: 10.1152/jn.91066.2008.
30. Yu XJ, Dickman JD, Angelaki DE. Detection thresholds of macaque otolith afferents. *J Neurosci* (2012) 32(24):8306-16. doi: 10.1523/JNEUROSCI.1067-12.2012.
31. Paulin MG, Hoffman LF. Models of vestibular semicircular canal afferent neuron firing activity. *J Neurophysiol* (2019) 122(6):2548-67. Epub 2019/11/07. doi: 10.1152/jn.00087.2019.
32. Baird RA, Desmadryl G, Fernández C, Goldberg JM. The vestibular nerve of the chinchilla. II. Relation between afferent response properties and peripheral innervation patterns in the semicircular canals. *J Neurophysiol* (1988) 60(1):182-203. Epub 1988/07/01.
33. Brichta AM, Goldberg JM. Morphological identification of physiologically characterized afferents innervating the turtle posterior crista. *J Neurophysiol* (2000) 83(3):1202-23. Epub 2000/03/11.
34. Fernández C, Baird RA, Goldberg JM. The vestibular nerve of the chinchilla. I. Peripheral innervation patterns in the horizontal and superior semicircular canals. *J Neurophysiol* (1988) 60(1):167-81. Epub 1988/07/01.

35. Fernandez C, Lysakowski A, Goldberg JM. Hair-cell counts and afferent innervation patterns in the cristae ampullares of the squirrel monkey with a comparison to the chinchilla. *J Neurophysiol* (1995) 73(3):1253-69. Epub 1995/03/01.
36. Brichta AM, Peterson EH. Vestibular afferents innervating the posterior ampullae in a turtle, Pseudemys scripta. *Ann N Y Acad Sci* (1992) 656:914-6.
37. Brichta AM, Peterson EH. Functional architecture of vestibular primary afferents from the posterior semicircular canal of a turtle, Pseudemys (Trachemys) scripta elegans. *J Comp Neurol* (1994) 344(4):481-507. doi: 10.1002/cne.903440402.
38. Schessel DA, Highstein SM. Is transmission between the vestibular type I hair cell and its primary afferent chemical? *Ann N Y Acad Sci* (1981) 374:210-4.
39. Contini D, Price SD, Art JJ. Accumulation of K+ in the synaptic cleft modulates activity by influencing both vestibular hair cell and calyx afferent in the turtle. *J Physiol* (2017) 595.3(3):777-803. doi: 10.1113/JP273060.
40. Brichta AM, Aubert A, Eatock RA, Goldberg JM. Regional analysis of whole cell currents from hair cells of the turtle posterior crista. *J Neurophysiol* (2002) 88(6):3259-78. Epub 2002/12/06. doi: 10.1152/jn.00770.2001.
41. Dickman JD, Correia MJ. Responses of Pigeon Horizontal Semicircular Canal Afferent Fibers II. High-Frequency Mechanical Stimulation. *J Neurophysiol* (1989) 62(5):1102-12.
42. Curthoys IS, Grant JW. How does high-frequency sound or vibration activate vestibular receptors? *Exp Brain Res* (2015) 233(3):691-9. doi: 10.1007/s00221-014-4192-6.
43. Schessel DA, Ginzberg R, Highstein SM. Morphophysiology of synaptic transmission between type I hair cells and vestibular primary afferents. An intracellular study employing horseradish peroxidase in the lizard, Calotes versicolor. *Brain Res* (1991) 544(1):1-16.
44. Goldberg JM, Baird RA, Fernández C. Morphophysiological studies of the mammalian vestibular labyrinth. *Prog Clin Biol Res* (1985) 176:231-45. Epub 1985/01/01.
45. Fernández C, Goldberg JM, Baird RA. The vestibular nerve of the chinchilla. III. Peripheral innervation patterns in the utricular macula. *J Neurophysiol* (1990) 63(4):767-80. Epub 1990/04/01.
46. Goldberg JM, Desmadryl G, Baird RA, Fernández C. The vestibular nerve of the chinchilla. V. Relation between afferent discharge properties and peripheral innervation patterns in the utricular macula. *J Neurophysiol* (1990) 63(4):791-804. Epub 1990/04/01.
47. Goldberg JM, Desmadryl G, Baird RA, Fernández C. The vestibular nerve of the chinchilla. IV. Discharge properties of utricular afferents. *J Neurophysiol* (1990) 63(4):781-90. Epub 1990/04/01.
48. Fernández C, Goldberg JM. Physiology of peripheral neurons innervating semicircular canals of the squirrel monkey. II. Response to sinusoidal stimulation and dynamics of peripheral vestibular system. *J Neurophysiol* (1971) 34(4):661-75. Epub 1971/07/01.
49. Goldberg JM, Fernández C. Physiology of peripheral neurons innervating semicircular canals of the squirrel monkey. 3. Variations among units in their discharge properties. *J Neurophysiol* (1971) 34(4):676-84. Epub 1971/07/01.
50. Goldberg JM, Fernández C. Physiology of peripheral neurons innervating semicircular canals of the squirrel monkey. I. Resting discharge and response to constant angular accelerations. *J Neurophysiol* (1971) 34(4):635-60. Epub 1971/07/01.

51. Curthoys IS. The response of primary horizontal semicircular canal neurons in the rat and guinea pig to angular acceleration. *Exp Brain Res* (1982) 47(2):286-94. Epub 1982/01/01. doi: 10.1007/BF00239388.
52. Brichta AM, Goldberg JM. Responses to efferent activation and excitatory response-intensity relations of turtle posterior-crista afferents. *J Neurophysiol* (2000) 83(3):1224-42. Epub 2000/03/11.
53. Art JJ. Comparative physiology of primary afferents innervating semicircular canals in two species of plethodontid salamanders [Dissertation]: University of Chicago (1979).
54. McCue MP, Guinan JJ, Jr. Acoustically responsive fibers in the vestibular nerve of the cat. *J Neurosci* (1994) 14(10):6058-70.
55. Curthoys IS, Burgess AM, Goonetilleke SC. Phase-locking of irregular guinea pig primary vestibular afferents to high frequency (>250Hz) sound and vibration. *Hear Res* (2019) 373:59-70. Epub 2019/01/02. doi: 10.1016/j.heares.2018.12.009.
56. Poppi LA, Holt JC, Lim R, Brichta AM. A review of efferent cholinergic synaptic transmission in the vestibular periphery and its functional implications. *J Neurophysiol* (2019). Epub 2019/12/05. doi: 10.1152/jn.00053.2019.
57. Holt JC, Jordan PM, Lysakowski A, Shah A, Barsz K, Contini D. Muscarinic Acetylcholine Receptors and M-Currents Underlie Efferent-Mediated Slow Excitation in Calyx-Bearing Vestibular Afferents. *J Neurosci* (2017) 37(7):1873-87. doi: 10.1523/JNEUROSCI.2322-16.2017.
58. Holt JC, Kewin K, Jordan PM, Cameron P, Klapczynski M, McIntosh JM, et al. Pharmacologically distinct nicotinic acetylcholine receptors drive efferent-mediated excitation in calyx-bearing vestibular afferents. *J Neurosci* (2015) 35(8):3625-43. Epub 2015/02/27. doi: 10.1523/jneurosci.3388-14.2015.
59. Jordan PM, Parks XX, Contini D, Holt JC. A review of synaptic mechanisms of vestibular efferent signaling in turtles: extrapolation to efferent actions in mammals. *J Vestib Res* (2013) 23(3):161-75. Epub 2013/11/02. doi: 10.3233/ves-130492.
60. Raghu V, Salvi R, Sadeghi SG. Efferent Inputs Are Required for Normal Function of Vestibular Nerve Afferents. *J Neurosci* (2019) 39(35):6922-35. Epub 2019/07/10. doi: 10.1523/JNEUROSCI.0237-19.2019.
61. Holstein GR, Rabbitt RD, Martinelli GP, Friedrich VL, Jr., Boyle RD, Highstein SM. Convergence of excitatory and inhibitory hair cell transmitters shapes vestibular afferent responses. *Proc Natl Acad Sci U S A* (2004) 101(44):15766-71. doi: 10.1073/pnas.0402824101.
62. Holstein GR, Martinelli GP, Henderson SC, Friedrich VL, Jr., Rabbitt RD, Highstein SM. Gamma-aminobutyric acid is present in a spatially discrete subpopulation of hair cells in the crista ampullaris of the toadfish Opsanus tau. *J Comp Neurol* (2004) 471(1):1-10. doi: 10.1002/cne.11025.
63. Highstein SM, Rabbitt RD, Holstein GR, Boyle RD. Determinants of spatial and temporal coding by semicircular canal afferents. *J Neurophysiol* (2005) 93(5):2359-70. doi: 10.1152/jn.00533.2004.
64. Contini D, Holstein GR, Art JJ. Synaptic cleft microenvironment influences potassium permeation and synaptic transmission in hair cells surrounded by calyx afferents in the turtle. *J Physiology* (2020) 598.4(4):853-89. Epub 2019/10/18. doi: 10.1113/JP278680.

528 65. Highstein SM, Holstein GR, Mann MA, Rabbitt RD. Evidence that protons act as
529 neurotransmitters at vestibular hair cell-calyx afferent synapses. *Proc Natl Acad Sci U S A* (2014)
530 111(14):5421-6. doi: 10.1073/pnas.1319561111.
531 66. Chen JW, Eatock RA. Major potassium conductance in type I hair cells from rat semicircular
532 canals: characterization and modulation by nitric oxide. *J Neurophysiol* (2000) 84(1):139-51.
533 67. Ross MD, Rogers CM, Donovan KM. Innervation patterns in rat saccular macula. A structural
534 basis for complex sensory processing. *Acta Otolaryngol* (1986) 102(1-2):75-86. Epub
535 1986/07/01. doi: 10.3109/00016488609108649.
536 68. Valat J, Devau G, Dulon D, Sans A. Vestibular hair cells isolated from guinea pig labyrinth.
537 *Hear Res* (1989) 40(3):255-60. Epub 1989/07/01.
538 69. Masetto S, Russo G, Taglietti V, Prigioni I. [K+ and Ca++ currents in hair cells isolated from
539 the semicircular canals of the frog]. *Boll Soc Ital Biol Sper* (1991) 67(5):493-500.
540 70. Rennie KJ, Ashmore JF. Ionic currents in isolated vestibular hair cells from the guinea-pig
541 crista ampullaris. *Hear Res* (1991) 51:279-92.
542 71. Prigioni I, Masetto S, Russo G, Taglietti V. Calcium currents in solitary hair cells isolated
543 from frog crista ampullaris. *J Vestib Res* (1992) 2(1):31-9.
544 72. Griguer C, Kros CJ, Sans A, Lehouelleur J. Potassium currents in type II vestibular hair cells
545 isolated from the guinea-pig's crista ampullaris [published erratum appears in Pflugers Arch
546 1994 May;427(1-2):193]. *Pflugers Archiv European Journal of Physiology* (1993) 425(3-4):344-
547 52.
548 73. Griguer C, Sans A, Lehouelleur J. Non-typical K(+)-current in cesium-loaded guinea pig type I
549 vestibular hair cell. *Pflugers Archiv European Journal of Physiology* (1993) 422(4):407-9.
550 74. Griguer C, Sans A, Valmier J, Lehouelleur J. Inward potassium rectifier current in type I
551 vestibular hair cells isolated from guinea pig. *Neurosci Lett* (1993) 149(1):51-5.
552 75. Lapeyre PN, Kolston PJ, Ashmore JF. GABAB-mediated modulation of ionic conductances in
553 type I hair cells isolated from guinea-pig semicircular canals. *Brain Res* (1993) 609(1-2):269-76.
554 76. Rennie KJ, Ashmore JF. Effects of extracellular ATP on hair cells isolated from the guinea-pig
555 semicircular canals. *Neurosci Lett* (1993) 160(2):185-9.
556 77. Rennie KJ, Correia MJ. Potassium currents in mammalian and avian isolated type I
557 semicircular canal hair cells. *J Neurophysiol* (1994) 71(1):317-29. Epub 1994/01/01.
558 78. Ricci AJ, Cochran SL, Rennie KJ, Correia MJ. Vestibular type I and type II hair cells. 2:
559 Morphometric comparisons of dissociated pigeon hair cells. *J Vestib Res* (1997) 7(5):407-20.
560 Epub 1997/11/05.
561 79. Ricci AJ, Rennie KJ, Cochran SL, Kevetter GA, Correia MJ. Vestibular type I and type II hair
562 cells. 1: Morphometric identification in the pigeon and gerbil. *J Vestib Res* (1997) 7(5):393-406.
563 Epub 1997/11/05.
564 80. Eatock RA, Rusch A, Lysakowski A, Saeki M. Hair cells in mammalian utricles. *Otolaryngol*
565 *Head Neck Surg* (1998) 119(3):172-81.
566 81. Marcotti W, Russo G, Prigioni I. Inactivating and non-activating delayed rectifier K+ currents
567 in hair cells of frog crista ampullaris. *Hear Res* (1999) 135(1-2):113-23.
568 82. Martini M, Rossi ML, Rubbini G, Rispoli G. Calcium currents in hair cells isolated from
569 semicircular canals of the frog. *Biophys J* (2000) 78(3):1240-54. doi: 10.1016/S0006-
570 3495(00)76681-1.

571 83. Rennie KJ, Weng T, Correia MJ. Effects of KCNQ channel blockers on K(+) currents in
572 vestibular hair cells. *Am J Physiol Cell Physiol* (2001) 280(3):C473-80. Epub 2001/02/15.
573 84. Li GQ, Meredith FL, Rennie KJ. Development of K(+) and Na(+) conductances in rodent
574 postnatal semicircular canal type I hair cells. *Am J Physiol Regul Integr Comp Physiol* (2010)
575 298(2):R351-8. doi: 10.1152/ajpregu.00460.2009.
576 85. Meredith FL, Benke TA, Rennie KJ. Hyperpolarization-activated current (I(h)) in vestibular
577 calyx terminals: characterization and role in shaping postsynaptic events. *J Assoc Res*
578 *Otolaryngol* (2012) 13(6):745-58. doi: 10.1007/s10162-012-0342-3.
579 86. Mann SE, Johnson M, Meredith FL, Rennie KJ. Inhibition of K+ currents in type I vestibular
580 hair cells by gentamicin and neomycin. *Audiol Neurootol* (2013) 18(5):317-26. doi:
581 10.1159/000354056.
582 87. Lewis RS, Hudspeth AJ. Voltage- and ion-dependent conductances in solitary vertebrate
583 hair cells. *Nature* (1983) 304(5926):538-41. Epub 1983/08/11.
584 88. Lewis RS, Hudspeth AJ. Frequency tuning and ionic conductances in hair cells of the
585 bullfrog's sacculus. In: Klinke R, Hartmann R, editors. *Hearing-Physiological Bases and*
586 *Psychophysics*. Berlin: Springer-Verlag (1983). p. 17-24.
587 89. Hudspeth AJ, Lewis RS. A model for electrical resonance and frequency tuning in saccular
588 hair cells of the bull-frog, Rana catesbeiana. *J Physiol* (1988) 400:275-97. Epub 1988/06/01.
589 90. Hudspeth AJ, Lewis RS. Kinetic analysis of voltage- and ion-dependent conductances in
590 saccular hair cells of the bull-frog, Rana catesbeiana. *J Physiol* (1988) 400:237-74. Epub
591 1988/06/01.
592 91. Art JJ, Fettiplace R. Variation of membrane properties in hair cells isolated from the turtle
593 cochlea. *J Physiol* (1987) 385:207-42. Epub 1987/04/01.
594 92. Art JJ, Crawford AC, Fettiplace R. Electrical resonance and membrane currents in turtle
595 cochlear hair cells. *Hear Res* (1986) 22:31-6. Epub 1986/01/01.
596 93. Smotherman MS, Narins PM. The electrical properties of auditory hair cells in the frog
597 amphibian papilla. *J Neurosci* (1999) 19(13):5275-92.
598 94. Meredith FL, Rennie KJ. Channeling your inner ear potassium: K(+) channels in vestibular
599 hair cells. *Hear Res* (2016). doi: 10.1016/j.heares.2016.01.015.
600 95. Chen W-Y. The Properties and Functions of a Low-Voltage Activated K(+) Current in Type I
601 Hair Cells of Rat Semicircular Canal Organs [Dissertation]. Rochester, NY: University of
602 Rochester (1995).
603 96. Frankenhaeuser B, Hodgkin AL. The after-effects of impulses in the giant nerve fibres of
604 Loligo. *J Physiol* (1956) 131(2):341-76.
605 97. Goldberg JM. Transmission between the type I hair cell and its calyx ending. *Ann N Y Acad*
606 *Sci - New Directions in Vestibular Research* (1996) 781:474-88. Epub 1996/06/19.
607 98. Goldberg JM. Theoretical analysis of intercellular communication between the vestibular
608 type I hair cell and its calyx ending. *J Neurophysiol* (1996) 76(3):1942-57. Epub 1996/09/01.
609 99. Arvanitaki A. Effects evoked in an axon by the activity of a contiguous one. *J Neurophysiol*
610 (1942) 5(2):89-108. doi: 10.1152/jn.1942.5.2.89.
611 100. Katz B, Schmitt OH. Electric interaction between two adjacent nerve fibres. *J Physiol*
612 (1940) 97(4):471-88.

613 101. Kramer RH, Davenport CM. Lateral Inhibition in the Vertebrate Retina: The Case of the
614 Missing Neurotransmitter. *PLoS Biol* (2015) 13(12):e1002322. Epub 2015/12/15. doi:
615 10.1371/journal.pbio.1002322.
616 102. Govindaraju AC, Quraishi IH, Lysakowski A, Eatock RA, Raphael RM. A Biophysical Model of
617 Nonquantal Transmission at the Vestibular Hair Cell-Calyx Synapse: K(LV) currents Modulate
618 Fast Electrical and Slow K(+) potentials in the Synaptic Cleft. *bioRxiv* (2021):2021.11.18.469197.
619 doi: 10.1101/2021.11.18.469197.
620 103. Holt JC, Chatlani S, Lysakowski A, Goldberg JM. Quantal and nonquantal transmission in
621 calyx-bearing fibers of the turtle posterior crista. *J Neurophysiol* (2007) 98(3):1083-101. Epub
622 2007/06/29. doi: 10.1152/jn.00332.2007.
623 104. Contini D. Intercellular K+ accumulation drives Type I hair cells into the activation range of
624 voltage-gated Ca channels [Dissertation]. Pavia, Italy: University of Pavia (2011).
625 105. Contini D, Zampini V, Tavazzani E, Magistretti J, Russo G, Prigioni I, et al. Intercellular K(+)
626 accumulation depolarizes Type I vestibular hair cells and their associated afferent nerve calyx.
627 *Neuroscience* (2012) 227:232-46. doi: 10.1016/j.neuroscience.2012.09.051.
628 106. Lim R, Kindig AE, Donne SW, Callister RJ, Brichta AM. Potassium accumulation between
629 type I hair cells and calyx terminals in mouse crista. *Exp Brain Res* (2011) 210(3-4):607-21. Epub
630 2011/02/26. doi: 10.1007/s00221-011-2592-4.
631 107. Eatock RA, Songer JE. Vestibular hair cells and afferents: two channels for head motion
632 signals. *Annu Rev Neurosci* (2011) 34:501-34. doi: 10.1146/annurev-neuro-061010-113710.
633 108. Songer JE, Eatock RA. Tuning and timing in mammalian type I hair cells and calyceal
634 synapses. *J Neurosci* (2013) 33(8):3706-24. Epub 2013/02/22. doi: 10.1523/jneurosci.4067-
635 12.2013.
636 109. Ireland J. *The Udana & The Itivuttaka: Inspired Utterances of the Buddha & The Buddha's*
637 *Sayings*: BPS Pariyatti Editions (2020).
638 110. Eatock RA. Specializations for Fast Signaling in the Amniote Vestibular Inner Ear. *Integr*
639 *Comp Biol* (2018) 58(2):341-50. Epub 2018/06/20. doi: 10.1093/icb/icy069.
640 111. McCue MP, Guinan JJ, Jr. Sound-evoked activity in primary afferent neurons of a
641 mammalian vestibular system. *Am J Otol* (1997) 18(3):355-60.
642 112. McCue MP, Guinan JJ, Jr. Spontaneous activity and frequency selectivity of acoustically
643 responsive vestibular afferents in the cat. *J Neurophysiol* (1995) 74(4):1563-72.
644 113. McCue MP, Guinan JJ, Jr. Influence of efferent stimulation on acoustically responsive
645 vestibular afferents in the cat. *J Neurosci* (1994) 14(10):6071-83. Epub 1994/10/01.
646 114. Curthoys IS, Vulovic V. Vestibular primary afferent responses to sound and vibration in the
647 guinea pig. *Exp Brain Res* (2011) 210(3-4):347-52. doi: 10.1007/s00221-010-2499-5.
648 115. Curthoys IS, Vulovic V, Sokolic L, Pogson J, Burgess AM. Irregular primary otolith afferents
649 from the guinea pig utricular and saccular maculae respond to both bone conducted vibration
650 and to air conducted sound. *Brain Res Bull* (2012) 89(1-2):16-21. doi:
651 10.1016/j.brainresbull.2012.07.007.
652 116. Curthoys IS, Vulovic V, Burgess AM, Sokolic L, Goonetilleke SC. The response of guinea pig
653 primary utricular and saccular irregular neurons to bone-conducted vibration (BCV) and air-
654 conducted sound (ACS). *Hear Res* (2016) 331:131-43. doi: 10.1016/j.heares.2015.10.019.

655 117. Highstein SM, Mann MA, Holstein GR, Rabbitt RD. The quantal component of synaptic
656 transmission from sensory hair cells to the vestibular calyx. *J Neurophysiol* (2015) 113(10):3827-
657 35. doi: 10.1152/jn.00055.2015.
658 118. Sadeghi SG, Pyott SJ, Yu Z, Glowatzki E. Glutamatergic signaling at the vestibular hair cell
659 calyx synapse. *J Neurosci* (2014) 34(44):14536-50. Epub 2014/10/31. doi:
660 10.1523/jneurosci.0369-13.2014.
661 119. Ramachandran S, Rodgriguez S, Potcoava M, Alford S. Single calcium channel
662 nanodomains drive presynaptic calcium entry at lamprey reticulospinal presynaptic terminals. *J*
663 *Neurosci* (2022). Epub 2022/01/23. doi: 10.1523/JNEUROSCI.2207-21.2022.
664 120. Art JJ, Wu YC, Fettiplace R. The calcium-activated potassium channels of turtle hair cells. *J*
665 *Gen Physiol* (1995) 105(1):49-72. Epub 1995/01/01.
666
667